Observation of pulsating aurora signatures in cosmic noise absorption data

M. Grandin,[1,2] A. Kero,[1] N. Partamies,[3] D. McKay,[1,4] D. Whiter,[5] A. Kozlovsky,[1] and Y. Miyoshi[6]

Keypoint #1: Cosmic noise absorption and blue-line auroral emission are strongly correlated during pulsating aurora event

Keypoint #2: Individual pulsations can be detected in cosmic noise absorption data and are consistent with the optical pulsations

Keypoint #3: This suggests that precipitation of both auroral and energetic electrons was modulated during the studied pulsating aurora event

Corresponding author: M. Grandin, Sodankylä Geophysical Observatory, Tähteläntie 62, FI-99600 Sodankylä, Finland. (maxime.grandin@sgo.fi)

[1]University of Oulu, Sodankylä Geophysical Observatory, Sodankylä, Finland

[2]Université de Toulouse; UPS-OMP; IRAP; Toulouse, France

[3]University Centre in Svalbard/Birkeland Centre for Space Science, Longyearbyen, Norway

[4]Department of Physics and Technology, University of Tromsø, Tromsø, Norway

[5]Space Environment Physics, University of Southampton, Southampton, United Kingdom

[6]Institute for Space-Earth Environmental Research, Nagoya University, Nagoya 464-8601, Japan

This study investigates the contribution of energetic ($E > 30$ keV) particle precipitation during a pulsating aurora event over Kilpisjärvi ($L = 6.2$) on 26 February 2014. It is based on the comparison of auroral blue-line emission (427.8 nm) data from an all-sky camera and cosmic noise absorption (CNA) data obtained from a multi-beam experiment of the Kilpisjärvi Atmospheric Imaging Receiver Array (KAIRA) riometer. The data sets are compared for three KAIRA beams close to magnetic zenith. Results show a clear correlation between the measured CNA and the auroral blue-line emission during the event, for each beam. In addition, individual pulsations are observed for the first time in the cosmic noise absorption data measured by KAIRA, and are found to be close-to-identical to the optical pulsations. This suggests that the modulation of electron precipitation during pulsating aurora takes place in a consistent way over a broad range of energies.

1. Introduction

Pulsating aurora is a frequently-observed form of the aurora borealis during which the light intensity exhibits on and off times across the sky. It may present various types of structures, such as arcs, arc segments or patches [*Davis*, 1978]. It is often observed in the equatorial part of the auroral oval during morning hours in magnetic local time, and may sometimes even take place throughout the whole latitudinal extent of the oval [*Kvifte and Pettersen*, 1969]. Although it is most commonly observed during the recovery phase of substorms, pulsating aurora may occur prior to a substorm and persist longer than its recovery phase [*Jones et al.*, 2011, 2013]. Pulsating structures may exhibit a wide range of time periods, from 2 s to 20 s [*Jaynes et al.*, 2015], the average being of the order of 8 ± 2 s [*Johnstone*, 1978]. An internal modulation of the auroral emission at 3 Hz is embedded in the main pulsations [*Sandahl et al.*, 1980; *Miyoshi et al.*, 2015a; *Nishiyama et al.*, 2016]. The pulsating patches are not necessarily in phase with each other and may have different periods [e.g., *Johnstone*, 1978; *Smith et al.*, 1980]. Generally, the fluctuations are characterized by quasiperiodic on and off times [*Humberset et al.*, 2016]. In addition, the pulsating structures tend to have an east-west drift at about 1 km/s [*Davis*, 1978].

It has been reported in many studies that pulsating aurora takes place over a diffuse background [e.g., *Royrvik and Davis*, 1977; *Jaynes et al.*, 2015]. The altitude of the pulsating aurora is generally comprised between 82 and 105 km [*Brown et al.*, 1976]. The intensity of the pulsating emission ranges from a few hundred Rayleigh (R) to a few kR [*Royrvik and Davis*, 1977].

The mechanism responsible for the modulation of auroral emission during pulsating aurora is still subject to discussion. It is commonly agreed that the scattering of electrons into the loss cone by very low frequency (VLF) waves in the near-equatorial region of the magnetosphere is involved [*Jaynes et al.*, 2013]. Likely candidates for the scattering waves are lower-band chorus waves [*Nishimura et al.*, 2011; *Miyoshi et al.*, 2010, 2015a], but the cause of the observed precipitating flux modulations is still debated. The possible mechanisms of periodic modulations have been debated, while theories such as non-linear relaxation oscillator [*Davidson*, 1986] and flow cyclotron maser [*Demekhov and Trakhtengerts*, 1994] have been suggested, among others.

The energies of precipitating electrons producing pulsating aurora typically range from a few keV to a few tens of keV [*Bryant et al.*, 1975; *McEwen et al.*, 1981; *Yau et al.*, 1981]. Nevertheless, *Miyoshi et al.* [2015b] revealed a possible contribution of electrons with energies reaching up to 200 keV, which was confirmed by *Turunen et al.* [2016]. *Miyoshi et al.* [2010, 2015a] have proposed that chorus waves propagating along the field line can cause wide-energy electron precipitation because the resonant energy depends on the ratio of ambient plasma frequency and electron gyrofrequency. Therefore, it is expected that electrons across a wide energy range simultaneously precipitate into the atmosphere in association with pulsating aurora. It is known that energetic ($E > 30$ keV) electron precipitation may ionize the ionosphere down to the D region. One of the signatures of D-region ionization is cosmic noise absorption (CNA), which is measured with riometers [e.g., *Shain*, 1951; *Hargreaves*, 1969]. The cosmic radio noise is continuously measured by an antenna, and the obtained signal is then subtracted from a so-called quiet-day curve corresponding to the cosmic radio noise received during an ideal day with no disturbance in the ionospheric *D* region. When expressed in decibels (dB), CNA at a given radio wave frequency is approximately proportional to the total electron content in the *D* region [*Hargreaves*, 1969].

The relationship between pulsating aurora and cosmic noise absorption was the object of a few studies in the 1960s and 1970s. *Campbell and Leinbach* [1961] were among the first to report a simultaneous observation of auroral pulsations and ionospheric absorption. Later on, several studies confirmed that pulsating aurora is often associated with cosmic noise absorption [e.g., *Berkey*, 1978; *Arnoldy et al.*, 1982]. On the other hand, *Brekke* [1971] made a statistical survey on the occurrence of pulsating aurora and cosmic noise absorption above Tromsø, and concluded that these phenomena are "completely independent" and do not necessarily occur simultaneously. Since then, both optical instruments and riometers have become significantly more advanced, thus enabling to study pulsating aurora in more detail, and especially at higher time resolution.

The objective of this study is to investigate whether pulsating aurora signatures can be detected in CNA, and if so, to compare their spatio-temporal characteristics to those which can be seen in optical data. The interest is to assess whether a given pulsating structure seen in the optical data exhibits the same pulsating period in riometer data, which would imply that the precipitation not only contains a broad range of energies but is also modulated simultaneously over these energies. For this purpose, we make use of the Kilpisjärvi Atmospheric Imaging Receiver Array (KAIRA), which may be utilized as a multibeam riometer with high signal-to-noise ratio, alongside a colocated all-sky camera providing optical data. While the optical data give information on electron precipitation in the 1–20 keV energy range, approximately, KAIRA is sensitive to > 30 keV electron precipitation. This paper focuses on a pulsating aurora event which took place during the early hours of 26 February 2014 above northern Fennoscandia.

2. Data

2.1. Optical Data from the Kilpisjärvi All-Sky Camera

The optical data was obtained from an all-sky camera (ASC) with an electron multiplying charge coupled device (EMCCD) and optical filters, installed in Kilpisjärvi (KIL, geographic 69.1°N, 20.8°E; $L = 6.2$). This instrument is part of the MIRACLE (Magnetometers - Ionospheric Radars - All-sky Cameras Large Experiment) network, and is maintained by the Finnish Meteorological Institute [*Syrjäsuo et al.*, 1998; *Sangalli et al.*, 2011]. The ASC data used in this study consists of 512×512 pixel images in the 427.8 nm (blue) auroral emission line, which is associated with N_2^+ first negative (1N) emission, and which is prompt. The images are taken with an exposure time of 1 s at a cadence of 2 s, and are stored in 16-bit PNG files. No other wavelengths were recorded during this event.

Pre-processing of the images consisted of subtracting the dark level, estimated from the median value of the pixel counts over the four corners of the detector, unlit by the all-sky image. Image count values were then multiplied by the calibration number (4.41 R/count) for this instrument at the time of the event. Therefore, the results presented below express optical data in rayleigh. The all-sky cameras of the MIRACLE network are calibrated for every winter season using an intercalibrated integrating sphere light source [*Brändström et al.*, 2012].

2.2. Cosmic Noise Absorption Data from KAIRA

The Kilpisjärvi Atmospheric Imaging Receiver Array (KAIRA) consists of two arrays of antennas operating in the very high frequency (VHF) range [*McKay-Bukowski et al.*, 2015]. The Low-Band Antenna (LBA) array is made of 48 cross-dipole antennas measuring the cosmic radio noise at frequencies ranging between 17 and 59 MHz, thus enabling spectral riometry measurements [*Kero et al.*, 2014].

For this study, CNA was derived within three KAIRA beams, thereafter called beam 1, 2 and 3. These beams have been chosen because they are pointing in directions close to magnetic zenith (see Figure 1), and therefore provide nearly field-aligned observations, minimizing the offset due to the optical emission and CNA taking place at different altitudes along the same magnetic field line.

To reduce the KAIRA data into a simple time series, while maintaining the statistics provided by the full spectrum measurement, the cosmic radio noise absorption in a given beam was estimated at $f_0 = 30$ MHz by fitting a monomial $A_{\mathrm{dB}}(f) = A_{\mathrm{dB}}(f_0)\,(f/f_0)^{\alpha}$ to the absorption spectrum data at each instant of time in 1 s resolution. The obtained mean value for the fitted parameter α was 1.93 ± 0.14. This procedure resulted in a sufficiently high signal-to-noise ratio desired in searching for the faint undulations in the CNA related to the pulsating aurora (see orange lines in Figures 2 and 3).

2.3. Mapping of the KAIRA Beams on the ASC Images

The KAIRA beams were mapped to their corresponding area in the ASC images at the altitude of 100 km, which is a common value for the peak emission during pulsating aurora [*Kataoka et al.*, 2016; *Oyama et al.*, 2016]. The beam width corresponds to the beam full width at half maximum (−3 dB) at 30 MHz given by *McKay-Bukowski et al.* [2015]. Figure 1 shows the projection of beams 1, 2 and 3 on an all-sky image from KIL. The position of magnetic zenith (MZ) is indicated in the image; it is located within beam 2.

In order to compare the CNA measured by KAIRA and the optical data in the corresponding beam areas (containing about 2000 pixels each), a weighted-average of the light intensity measured by the pixels within each beam has been calculated. A parabolic function reaching its maximum at the center of the beam and dropping to 0 at the edge of the beam was chosen for the corresponding weights to give more importance to the center of the beam and thus better represent the sensitivity of KAIRA across the beam. The sum of the weights over the beam is equal to 1.

3. Results

3.1. Time Series Comparison

Figure 2 shows a comparison of both data sets for each beam, from 02:00 UT until 02:35 UT, which corresponds to the time interval during which pulsating structures were visible in the vicinity of the considered beams. A cross-correlation of the two data sets revealed a systematic time delay of about 4 s, with the KAIRA data leading the ASC data. This technical issue was reported in *Virtanen* [2012], and was corrected for by shifting the KAIRA data by 4 s in what follows, bearing in mind that this may eclipse potential delays of geophysical origin.

The top panels of Figure 2 display the data as time series, with the optical data in blue and the KAIRA data in orange. Optical and CNA data show very similar overall variations. This is confirmed by the very strong correlation appearing in the bottom panels, indicating that intense blue-line emission is generally coincident with high CNA values. The Pearson correlation coefficients have been calculated to be 0.907 for beam 1, 0.905 for beam 2, and 0.875 for beam 3. These high, similar values suggest that the same precipitation (although potentially in a different energy range) caused both the optical emission and the CNA.

The optical pulsations visible in Figure 2 occur on top of a background that varies between 400 R (beams 1 and 3, shortly after 02:00) and almost 700 R (beam 2, around 02:10). Correspondingly, the CNA values during pulsating aurora range between 0.2 and 0.6 dB.

Typical values for auroral blue-line emission during pulsating aurora are of the order of a few hundred R to kR [*Royrvik and Davis*, 1977]. This is much less than during the active phases of substorms, when the intensity may exceed 10 kR at 427.8 nm [*Borovkov et al.*, 2005]. CNA values typically exceed 0.5 dB during energetic particle precipitation, and may occasionally reach values as high as 10 dB. However, the pulsating aurora events studied by *Milan et al.* [2008] and recently *Turunen et al.* [2016], exhibit CNA of the order of 0.5–1 dB.

3.2. Superposed Epoch Analysis of Pulsations

In order to study more specifically the pulsating structures and search for potential signatures in CNA, for each beam, the time interval with clearest pulsation signatures in the optical data was identified: 02:04:30–02:07:40 UT for beam 1, 02:09:00–02:11:30 UT for beam 2, and 02:22:40–02:25:50 UT for beam 3. The top panels of Figure 3 show the time series of ASC (blue) and KAIRA (orange) data during those intervals.

To isolate the contribution of the pulsating aurora to emission intensity and CNA, the slowly-varying component of the signals has been removed using a high-pass filter. This was done using a Butterworth digital filter of order 3 and of cutting frequency 16.7 mHz (i.e., keeping frequencies corresponding to periods under 1 min). The filtered signals, whose variations are dominated by the pulsations, are shown in the bottom panels of Figure 3 (optical data in blue, CNA data in orange). At this stage, it can be noted that very clear pulsations in CNA are already visible in the case of beam 1 (bottom-left-hand panel), which furthermore match well with the pulsations in the corresponding optical data. Even beams 2 and 3 seem to exhibit CNA pulsations which might follow the optical fluctuations. Yet, to extract and compare the statistical characteristics of these fluctuations in both data sets, a superposed epoch analysis was carried out. The zero epochs for the superposed epoch analysis were chosen to correspond to the times when, for a given beam, the ASC data is about to increase sharply and significantly. In other words, zero epochs were set to the local brightness minima during the pulsating aurora. They are shown in Figure 3 with black stars in the bottom panels.

Results of the superposed epoch analysis are shown in Figure 4. In each panel, the red line corresponds to median values, and the blue lines give the upper and lower quartiles describing the variability in the data. The top panels show the statistical properties of the ASC data during pulsations, for beams 1, 2 and 3, from 14 seconds prior to zero epoch until 20 seconds after zero epoch. Based on the median curves, the average period of pulsations is about 12 s for beam 1, about 10 s for beam 2, and 8–10 s for beam 3. The clearest pulsations can be seen around the zero epoch, while features are generally less clear more than 10 s away from the zero epoch. This is probably due to the pulsations being fairly irregular in time period.

The bottom panels of Figure 4 show the same analysis made for the corresponding KAIRA data, using the same zero epochs as for the optical data. The curves, albeit noisier than the ones above, also show signatures of pulsations. These signatures are present both in the median and in the quartile curves, suggesting that the CNA fluctuations which were noted in Figure 3 are indeed associated with pulsating aurora. The overall variations of the KAIRA data curves are fairly similar to those of the corresponding ASC data curves. In particular, the periods of pulsations are of the same order, for each beam.

4. Discussion

A first point which must be discussed is the choices made for the beam mapping. Indeed, the retained beam width and parametrization of the ASC data might not perfectly match reality. As the pulsating structures drift in and out of the beams, inaccuracies in the beam mapping may create a mismatch when comparing the two data sets. However, it has been tested that (1) dividing the beam size by two, and (2) using the median pixel count within the beam for parametrization only marginally affects the results. Correlations, pulsating signatures and their periods remain unaffected by those changes. This gives confidence in the robustness of the approach, including to the effect of the drifting motion of the pulsating structures.

The analysis of Figure 2 underlines that there is not a typical emission intensity nor CNA value associated to the pulsating aurora phenomenon during this single event. However, blue-line emission and CNA do correlate with each other during events containing pulsating aurora. Two possible explanations might account for such a good correlation. First, the particle precipitation spectrum may contain energies ranging from a few keV to several tens of keV, with $E \simeq 10$ keV electrons causing the optical emission and $E > 30$ keV electrons being responsible for CNA. CNA would therefore mostly originate from the D region, about 10 km or more below the altitude where the optical emission takes place. However, given that the pulsation signatures in CNA are very small (peak-to-peak amplitude of the order of 0.1 dB for beam 1, 0.05 dB for beam 2, and 0.03 dB for beam 3, based on the bottom panels of Figure 3), the CNA modulation might also be related to electron density variations at the altitude of the 427.8 nm emission, in the lower E region. This would mean that the $E > 30$ keV part of the precipitating spectrum detected by CNA does not necessarily undergo the same modulation as the auroral energies.

We tested these two scenarios using the Sodankylä Ion-Neutral Chemistry (SIC) model to estimate the expected amplitude of CNA modulations produced during the pulsating aurora event. The SIC model is a one-dimensional coupled chemistry model of the middle atmosphere which includes the resolution of the continuity equation for ion and neutral species in the D region, taking into account production processes including solar extreme ultraviolet and X-ray radiation, particle precipitation, and galactic cosmic rays, and loss processes through several hundred reactions. A detailed description of the model may be found in *Verronen et al.* [2005]. The SIC model has a wide range of applications, including the study of the effects of energetic particle precipitation on the mesosphere and on the ionospheric D region, and was previously used in a recent pulsating aurora study [*Turunen et al.*, 2016]. A realistic ionization rate profile was first obtained by making use of measurements by the European Incoherent Scatter (EISCAT) Radar at the time of the pulsating aurora event. The EISCAT radar beam was located inside the field of view of the Kilpisjärvi ASC, and therefore observed pulsating structures during the event. The ionization rate profile used as an input for the SIC model was derived using the same method as in *Turunen et al.* [2016]. In the simulations, these ionization rates were modulated by 25% over a 10 s period (of the order of what is observed in beam 1, see Figure 3) across part or all of the altitude range (80–150 km), depending on the scenario.

We first tested the hypothesis in which the pulsating ionization would take place only in the E region down to 100 km, i.e., in the altitudes of pulsating optical emissions, whilst the D region would be under constant ionization. Results suggest that under those conditions the expected CNA modulation is an order of magnitude smaller than observed ($\approx$ 0.01 dB). On the other hand, modulating the ionization profile uniformly at all the altitudes between 80 and 150 km, i.e., including in the D region, results in a circa 0.1 dB modulation observed, comparable to observations in beam 1. Horizontal lines have been plotted in grey in the bottom panel of Figure 3 corresponding to beam 1 to show the results of these simulations. The dotted lines give the amplitude of the simulated CNA pulsations in the case of E-region ionization modulation only (at $\pm$0.0062 dB), while the dashed lines give the results of a uniform modulation of the ionization profile, including in the *D* region (at ±0.0560 dB). These considerations suggest that the precipitation related to the pulsating aurora is pulsating also in the energies > 30 keV, therefore favoring the scenario of one single population of precipitating electrons over a broad range of energies. This result is consistent with a model proposed by *Miyoshi et al.* [2010, 2015b], which shows wide-energy electron precipitation associated with the pulsating aurora due to chorus waves.

Within each considered KAIRA beam, the time interval exhibiting the clearest pulsations in the ASC data was selected to perform the superposed epoch analysis. While it has been highlighted that the characteristic period of pulsations differ from one beam to another (i.e., from one patch to another), it must also be pointed out that the period of pulsations of a single patch varies within timescales as short as a few minutes. This irregularity in optical pulsation period can be very clearly seen in the ASC data shown in Figure 3; it agrees with results obtained by *Humberset et al.* [2016] based on a study of pulsating patches observed with an all-sky imager on 1 March 2012 over Poker Flat (Alaska).

5. Summary

By comparing the 427.8 nm emission observed with the Kilpisjärvi ASC and the CNA in three KAIRA beams during a pulsating aurora event on 26 February 2014, it has been shown that there is a clear correlation between these two parameters. This is evidence that the electron precipitation flux in energies above 30 keV related to the pulsating aurora event is subject to close-to-identical variations as that observed in the optical emissions.

In addition, signatures of pulsations in the CNA data have been observed, and confirmed by applying the superposed epoch method to subsets of the data exhibiting clear pulsation signatures in the optical data. This indicates that the D-region electron density variations are subject to forcing by the energetic electron precipitation which exhibits on and off times. The mechanism responsible for the ∼10 s precipitation modulation seems to affect the auroral (1–20 keV) and energetic ($>$ 30 keV) parts of the spectrum in a close-to-similar way.

This study shows that it is possible to detect pulsating aurora even when optical data are not available, e.g., with cloudy conditions or during the polar summer. In particular, conjunctions between the Japanese Arase (ERG) satellite [*Miyoshi et al.*, 2012] and ground-based instruments in northern Fennoscandia in the post-midnight and morning MLT sectors could be exploited to study pulsating aurora even outside of the dark season, using KAIRA instead of the optical instruments. This may prove important to study the atmospheric effects of high-energy precipitation during pulsating aurora events, as was initiated by *Turunen et al.* [2016].

Acknowledgments. This work was supported by the International Space Science Institute (ISSI) in Bern, Switzerland. A. Kero was supported by European Regional Development Fund (Regional Council of Lapland, decision number A70179). N. Partamies was supported by the Norwegian Research Council (grant 223252). Y. Miyoshi was supported by a Grant-in-Aid for Scientific Research (15H051815, 15H05747, 16H06286) from MEXT, Japan. The Kilpisjärvi all-sky camera images were obtained from the MIRACLE database (`http://space.fmi.fi/MIRACLE/`). The authors thank all the people contributing to the annual operation, maintenance and calibration of the MIRACLE cameras. The KAIRA data come from the Sodankylä Geophysical Observatory database (`http://www.sgo.fi`). KAIRA was funded by the University of Oulu and the FP7 European Regional Development Fund and is operated by Sodankylä Geophysical Observatory.

References

Arnoldy, R. L., K. Dragoon, L. J. Cahill, Jr., S. B. Mende, and T. J. Rosenberg (1982), Detailed correlations of magnetic field and riometer observations at L = 4.2 with pulsating aurora, *J. Geophys. Res.*, *87*, 10,449–10,456, doi:10.1029/JA087iA12p10449.

Berkey, F. T. (1978), Observations of pulsating aurora in the day sector auroral zone, *Planet. Space Sci.*, *26*, 635–650, doi:10.1016/0032-0633(78)90097-1.

Borovkov, L. P., B. V. Kozelov, L. S. Yevlashin, and S. A. Chernouss (2005), Variations of auroral hydrogen emission near substorm onset, *Annales Geophysicae*, *23*, 1623–1635, doi:10.5194/angeo-23-1623-2005.

Brändström, B. U. E., C.-F. Enell, O. Widell, T. Hansson, D. Whiter, S. Mäkinen, D. Mikhaylova, K. Axelsson, F. Sigernes, N. Gulbrandsen, N. M. Schlatter, A. G. Gjendem, L. Cai, J. P. Reistad, M. Daae, T. D. Demissie, Y. L. Andalsvik, O. Roberts, S. Poluyanov, and S. Chernouss (2012), Results from the intercalibration of optical low light calibration sources 2011, *Geoscientific Instrumentation, Methods and Data Systems*, *1*(1), 43–51, doi:10.5194/gi-1-43-2012.

Brekke, A. (1971), On the correlation between pulsating aurora and cosmic radio noise absorption, *Planetary and Space Science*, *19*, 891–896, doi:10.1016/0032-0633(71)90140-1.

Brown, N. B., T. N. Davis, T. J. Hallinan, and H. C. Stenbaek-Nielsen (1976), Altitude of pulsating aurora determined by a new instrumental technique, *Geophys. Res. Lett.*, *3*, 403, doi:10.1029/GL003i007p00403.

Bryant, D. A., M. J. Smith, and G. M. Courtier (1975), Distant modulation of electron intensity during the expansion phase of an auroral substorm, *Planetary and Space Science*, *23*, 867–878, doi:10.1016/0032-0633(75)90022-7.

Campbell, W. H., and H. Leinbach (1961), Ionospheric Absorption at Times of Auroral and Magnetic Pulsations, *J. Geophys. Res.*, *66*, 25–34, doi:10.1029/JZ066i001p00025.

Davidson, G. T. (1986), Pitch angle diffusion in morningside aurorae: 2. the formation of repetitive auroral pulsations, *J. Geophys. Res. Space Physics*, *91*(A4), 4429–4436, doi:10.1029/JA091iA04p04429.

Davis, T. N. (1978), Observed characteristics of auroral forms, *Space Science Reviews*, *22*, 77–113, doi:10.1007/BF00215814.

Demekhov, A. G., and V. Y. Trakhtengerts (1994), A mechanism of formation of pulsating aurorae, *J. Geophys. Res. Space Physics*, *99*(A4), 5831–5841, doi:10.1029/93JA01804.

Hargreaves, J. K. (1969), Auroral absorption of HF radio waves in the ionosphere: A review of results from the first decade of riometry., *IEEE Proceedings*, *57*, 1348–1373.

Humberset, B. K., J. W. Gjerloev, M. Samara, R. G. Michell, and I. R. Mann (2016), Temporal characteristics and energy deposition of pulsating auroral patches, *J. Geophys. Res. Space Physics*, *121*(7), 7087–7107, doi:10.1002/2016JA022921, 2016JA022921.

Jaynes, A. N., M. R. Lessard, J. V. Rodriguez, E. Donovan, T. M. Loto'Aniu, and K. Rychert (2013), Pulsating auroral electron flux modulations in the equatorial magnetosphere, *Journal of Geophysical Research (Space Physics)*, *118*, 4884–4894, doi: 10.1002/jgra.50434.

Jaynes, A. N., M. R. Lessard, K. Takahashi, A. F. Ali, D. M. Malaspina, R. G. Michell, E. L. Spanswick, D. N. Baker, J. B. Blake, C. Cully, E. F. Donovan, C. A. Kletzing, G. D. Reeves, M. Samara, H. E. Spence, and J. R. Wygant (2015), Correlated Pc4-5 ULF waves, whistler-mode chorus, and pulsating aurora observed by the Van Allen Probes and ground-based systems, *J. Geophys. Res. Space Physics*, *120*, 8749–8761, doi:10.1002/2015JA021380.

Johnstone, A. D. (1978), Pulsating aurora, *Nature*, *274*, 119–126, doi:10.1038/274119a0.

Jones, S. L., M. R. Lessard, K. Rychert, E. Spanswick, and E. Donovan (2011), Large-scale aspects and temporal evolution of pulsating aurora, *J. Geophys. Res. Space Physics*, *116*, A03214, doi:10.1029/2010JA015840.

Jones, S. L., M. R. Lessard, K. Rychert, E. Spanswick, E. Donovan, and A. N. Jaynes (2013), Persistent, widespread pulsating aurora: A case study, *J. Geophys. Res. Space Physics*, *118*, 2998–3006, doi:10.1002/jgra.50301.

Kataoka, R., Y. Fukuda, H. A. Uchida, H. Yamada, Y. Miyoshi, Y. Ebihara, H. Dahlgren, and D. Hampton (2016), High-speed stereoscopy of aurora, *Annales Geophysicae*, *34*, 41–44, doi:10.5194/angeo-34-41-2016.

Kero, A., J. Vierinen, D. McKay-Bukowski, C.-F. Enell, M. Sinor, L. Roininen, and Y. Ogawa (2014), Ionospheric electron density profiles inverted from a spectral riometer measurement, *Geophys. Res. Lett.*, *41*, 5370–5375, doi:10.1002/2014GL060986.

Kvifte, G. J., and H. Pettersen (1969), Morphology of the pulsating aurora, *Planetary and Space Science*, *17*, 1599–1607, doi:10.1016/0032-0633(69)90148-2.

McEwen, D. J., E. Yee, B. A. Whalen, and A. W. Yau (1981), Electron energy measurements in pulsating auroras, *Canadian Journal of Physics*, *59*, 1106–1115, doi:10.1139/p81-146.

McKay-Bukowski, D., J. Vierinen, I. I. Virtanen, R. Fallows, M. Postila, T. Ulich, O. Wucknitz, M. Brentjens, N. Ebbendorf, C.-F. Enell, M. Gerbers, T. Grit, P. Gruppen, A. Kero, T. Iinatti, M. Lehtinen, H. Meulman, M. Norden, M. Orispää, T. Raita, J. P. de Reijer, L. Roininen, A. Schoenmakers, K. Stuurwold, and E. Turunen (2015), KAIRA: The Kilpisjärvi Atmospheric Imaging Receiver Array—System Overview and First Results, *IEEE Transactions on Geoscience and Remote Sensing*, *53*, 1440–1451, doi:10.1109/TGRS.2014.2342252.

Milan, S. E., K. Hosokawa, M. Lester, N. Sato, H. Yamagishi, and F. Honary (2008), D region HF radar echoes associated with energetic particle precipitation and pulsating aurora, *Annales Geophysicae*, *26*, 1897–1904, doi:10.5194/angeo-26-1897-2008.

Miyoshi, Y., Y. Katoh, T. Nishiyama, T. Sakanoi, K. Asamura, and M. Hirahara (2010), Time of flight analysis of pulsating aurora electrons, considering wave-particle interactions with propagating whistler mode waves, *J. Geophys. Res. Space Physics*, *115*, A10312, doi:10.1029/2009JA015127.

Miyoshi, Y., T. Ono, T. Takashima, K. Asamura, M. Hirahara, Y. Kasaba, A. Matsuoka, H. Kojima, K. Shiokawa, K. Seki, M. Fujimoto, T. Nagatsuma, C. Z. Cheng, Y. Kazama, S. Kasahara, T. Mitani, H. Matsumoto, N. Higashio, A. Kumamoto, S. Hagitani, Y. Kasahara, K. Ishisaka, L. Blomberg, A. Fujimoto, Y. Katoh, Y. Ebihara, Y. Omura, M. Nose, T. Hori, Y. Miyashita, Y. Tanaka, T. Segawa, and ERG working group (2012), The Energization and Radiation in Geospace (ERG) Project, in *Dynamics of the Earth's Radiation Belts and Inner Magnetosphere, Geophys. Monogr. Ser.*, vol. 199, edited by D. Summers, I. R. Mann, D. N. Baker, and M. Schulz, pp. 103–116, AGU, Washington D.C., doi:10.1029/2012BK001304.

Miyoshi, Y., S. Saito, K. Seki, T. Nishiyama, R. Kataoka, K. Asamura, Y. Katoh, Y. Ebihara, T. Sakanoi, M. Hirahara, S. Oyama, S. Kurita, and O. Santolik (2015a), Relation between fine structure of energy spectra for pulsating aurora electrons and frequency spectra of whistler mode chorus waves, *J. Geophys. Res. Space Physics*, *120*, 7728–7736, doi:10.1002/2015JA021562.

Miyoshi, Y., S. Oyama, S. Saito, S. Kurita, H. Fujiwara, R. Kataoka, Y. Ebihara, C. Kletzing, G. Reeves, O. Santolik, M. Clilverd, C. J. Rodger, E. Turunen, and F. Tsuchiya (2015b), Energetic electron precipitation associated with pulsating aurora: EISCAT and Van Allen Probe observations, *J. Geophys. Res. Space Physics*, *120*, 2754–2766, doi:10.1002/2014JA020690.

Nishimura, Y., J. Bortnik, W. Li, R. M. Thorne, L. Chen, L. R. Lyons, V. Angelopoulos, S. B. Mende, J. Bonnell, O. L. Contel, C. Cully, R. Ergun, and U. Auster (2011), Multievent study of the correlation between pulsating aurora and whistler mode chorus emissions, *J. Geophys. Res. Space Physics*, *116*(A11), doi:10.1029/2011JA016876.

Nishiyama, T., Y. Miyoshi, Y. Katoh, T. Sakanoi, R. Kataoka, and S. Okano (2016), Substructures with luminosity modulation and horizontal oscillation in pulsating patch:

Principal component analysis application to pulsating aurora, *J. Geophys. Res. Space Physics*, *121*, 2360–2373, doi:10.1002/2015JA022288.

Oyama, S.-I., K. Shiokawa, Y. Miyoshi, K. Hosokawa, B. J. Watkins, J. Kurihara, T. T. Tsuda, and C. T. Fallen (2016), Lower thermospheric wind variations in auroral patches during the substorm recovery phase, *J. Geophys. Res. Space Physics*, *121*, 3564–3577, doi:10.1002/2015JA022129.

Royrvik, O., and T. N. Davis (1977), Pulsating aurora - Local and global morphology, *J. Geophys. Res.*, *82*, 4720–4740, doi:10.1029/JA082i029p04720.

Sandahl, I., L. Eliasson, and R. Lundin (1980), Rocket observations of precipitating electrons over a pulsating aurora, *Geophys. Res. Lett.*, *7*, 309–312, doi:10.1029/GL007i005p00309.

Sangalli, L., N. Partamies, M. Syrjäsuo, C.-F. Enell, K. Kauristie, and S. Mäkinen (2011), Performance study of the new EMCCD-based all-sky cameras for auroral imaging, *International Journal of Remote Sensing*, *32*, 2987–3003, doi:10.1080/01431161.2010.541505.

Shain, C. A. (1951), Galactic Radiation at 18.3 Mc/s., *Australian Journal of Scientific Research A Physical Sciences*, *4*, 258, doi:10.1071/PH510258.

Smith, M. J., D. A. Bryant, and T. Edwards (1980), Pulsations in auroral electrons and positive ions, *Journal of Atmospheric and Terrestrial Physics*, *42*, 167–178.

Syrjäsuo, M., T. I. Pulkkinen, P. Janhunen, A. Viljanen, R. J. Pellinen, K. Kauristie, H. J. Opgenoorth, S. Wallman, P. Eglitis, P. Karlsson, O. Amm, E. Nielsen, and C. Thomas (1998), Observations of Substorm Electrodynamics Using the MIRACLE Network, in *Substorms-4*, *Astrophysics and Space Science Library*, vol. 238, edited by S. Kokubun and Y. Kamide, p. 111, doi:10.1007/978-0-7923-5465-9_23.

Turunen, E., A. Kero, P. T. Verronen, Y. Miyoshi, S.-I. Oyama, and S. Saito (2016), Mesospheric ozone destruction by high-energy electron precipitation associated with pulsating aurora, *J. Geophys. Res. Atmospheres*, *121*(19), 11,852–11,861, doi:10.1002/2016JD025015, 2016JD025015.

Verronen, P. T., A. Seppälä, M. A. Clilverd, C. J. Rodger, E. Kyrölä, C.-F. Enell, T. Ulich, and E. Turunen (2005), Diurnal variation of ozone depletion during the October-November 2003 solar proton events, *J. Geophys. Res. Space Physics*, *110*(A9), doi:10.1029/2004JA010932, A09S32.

Virtanen, I. I. (2012), Station Data Cookbook, *Tech. Rep. LOFAR-ASTRON-MAN-064*, ASTRON.

Yau, A. W., B. A. Whalen, and D. J. McEwen (1981), Rocket-borne measurements of particle pulsation in pulsating aurora, *J. Geophys. Res. Space Physics*, *86*(A7), 5673–5681, doi:10.1029/JA086iA07p05673.

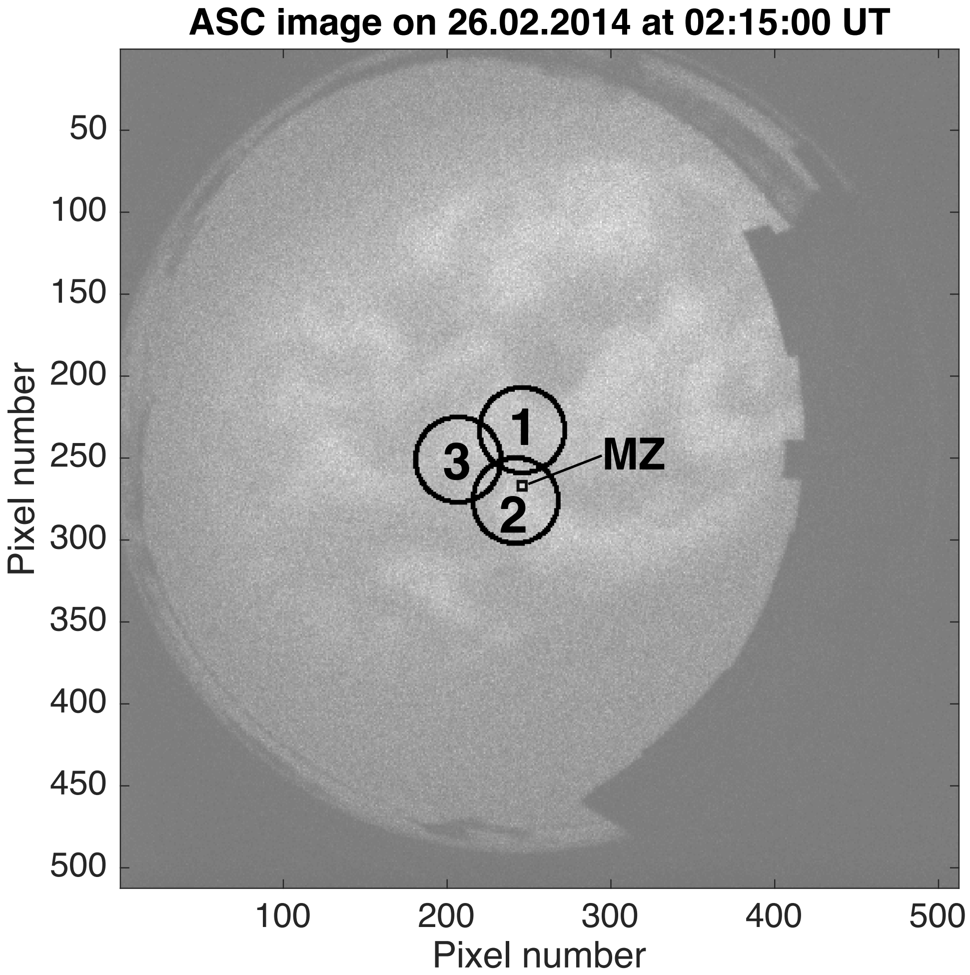

Figure 1. Position of the KAIRA beams number 1, 2 and 3 on an example KIL all-sky image. Magnetic zenith (MZ) is indicated inside beam 2.

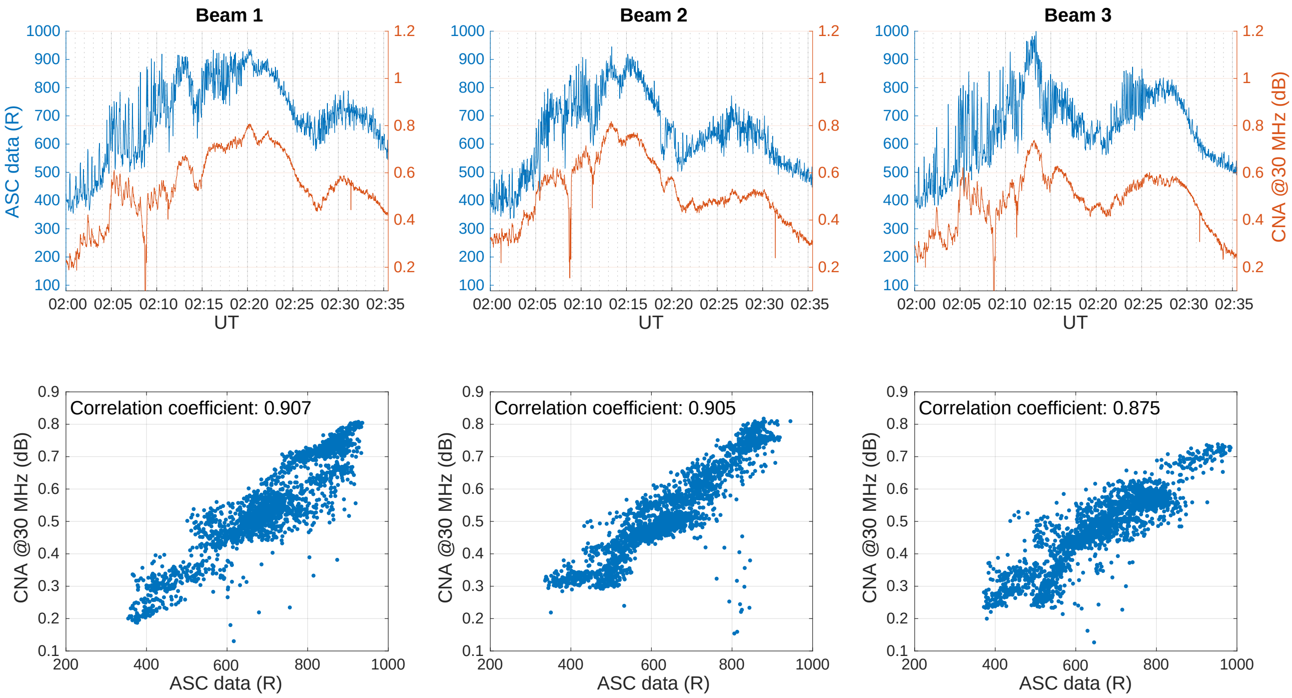

Figure 2. (top) Time series of the 427.8 nm auroral emission (blue) and cosmic noise absorption (orange) between 02:00 and 02:35 UT within KAIRA beams number 1, 2 and 3. (bottom) Correlation between cosmic noise absorption and 427.8 nm auroral emission within these same beams.

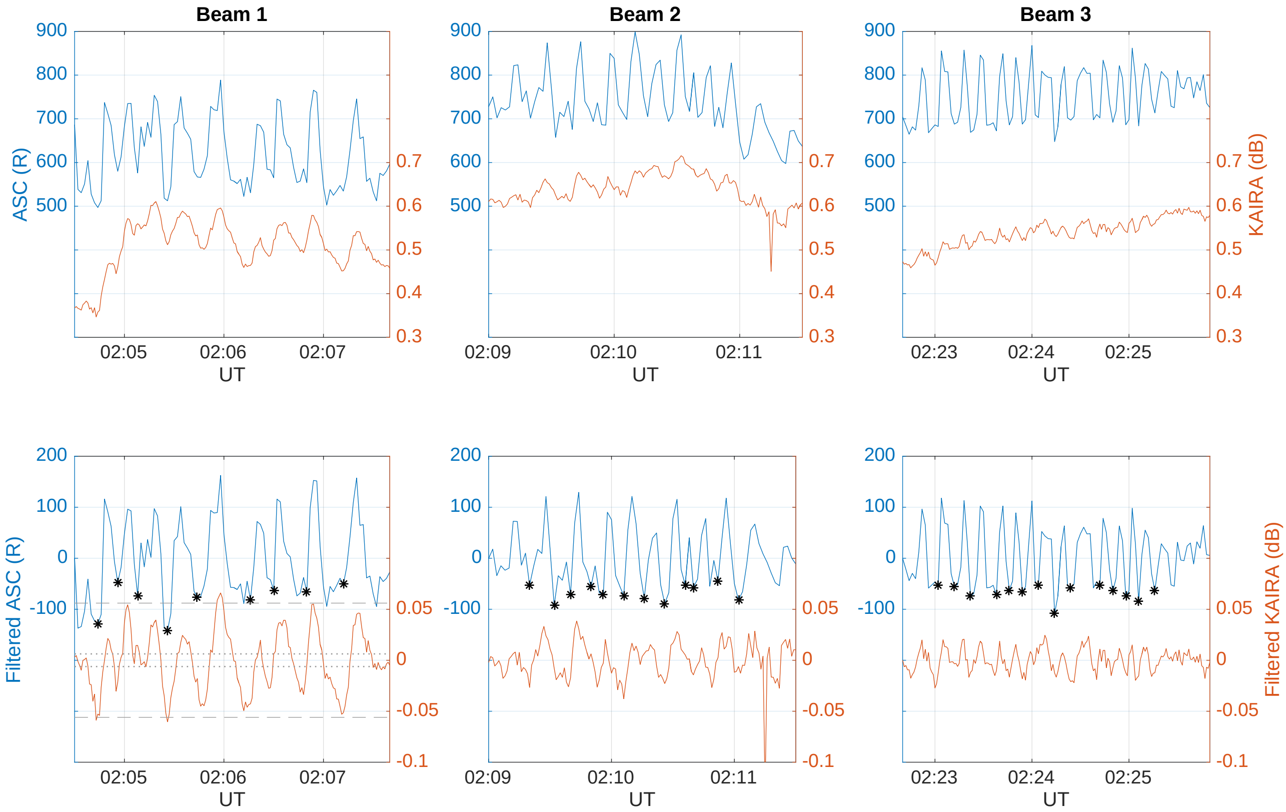

Figure 3. Time series of the data during pulsation time intervals in beams number 1, 2 and 3. (first row) Raw optical (blue) and CNA (orange) data. (second row) High-pass-filtered optical (blue) and CNA (orange) data. The black stars indicate zero epochs for the superposed epoch analysis. The horizontal grey lines in the bottom panel corresponding to beam 1 indicate the amplitude of the CNA pulsations simulated using the SIC model in the case of only E-region ionization modulation (dotted lines) and in the case of all ionization profile modulation, including in the D region (dashed lines) [see Discussion].

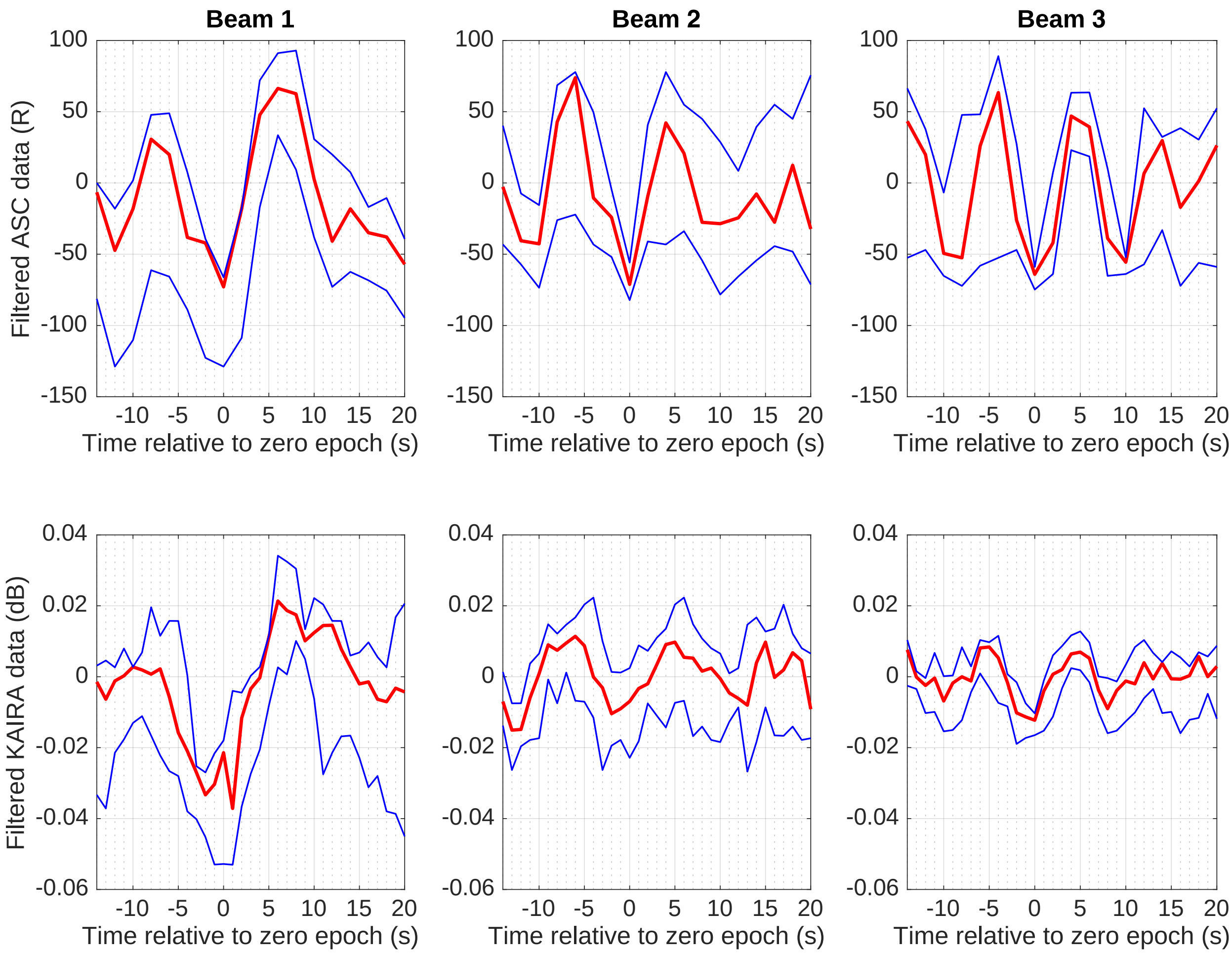

Figure 4. Superposed epoch analysis of pulsations in the optical (top panels) and absorption (bottom panels) data for beams number 1, 2 and 3. The red lines correspond to median values, while the blue lines correspond to the upper and lower quartiles.